TSINGHUA SCIENCE AND TECHNOLOGY
ISSN 1007-0214 20/20 pp127-132
Volume 15, Number 1, February 2010

Simulation of EUV Imaging and 3-D Cone-Beam CT Reconstruction on the Plasmasphere*

CHEN Zhiqiang (陈志强), ZHENG Jie (郑 杰), LI Liang (李 亮)**, XU Ronglan (徐荣栏)†, JIN Xin (金 鑫), HUANG Ya (黄 娅)†

Key Laboratory of Particle & Radiation Imaging of Ministry of Education, Department of Engineering Physics, Tsinghua University, Beijing 100084, China;
† Centre of Space and Applied Research, Chinese Academy of Sciences, Beijing 100190, China

Abstract: A three-dimensional (3-D) phantom for the density distribution of the plasmasphere is established . The imaging processes of the extreme ultraviolet (EUV) Imager are computer-simulated, in which the Earth shelter is treated as a main problem. A modified ART method is devised to resolve the incomplete data reconstruction problem to validate and evaluate the proposed methods. The cone-beam EUV data are simulated based on the 3-D phantom from both a circular and semi-circular trajectories. Quantitative reconstruction results demonstrate the correctness of the proposed modified ART algorithm. The CT technique can be used to calculate the global density of the plasmasphere from the EUV data.

Key words: computed tomography (CT); plasmasphere; extreme ultraviolet (EUV); ART algorithm

Introduction

The earth plasmasphere is a region within 4 Re (radius of the earth) from the earth center, consisting of cold charged particles having the kinetic energy of about 1 eV. The plamasphere may influence the control and security of spacecraft which should be given adequate attention. Since the data from in situ measurement of plasmasphere density along a spacecraft trajectory cannot help distinguish the variation due to the space or time variation, the nearly instantaneous measurement of its topology is required[1,2]. Under solar radiation, the He^+ ion, constituting of 20% of the plasma population resonantly scatters isotropic EUV (extreme ultraviolet) radiation with the wavelength of 30.4 nm, while H^+, taking the remaining part, has no optical emission. The brightness of the 30.4 nm feature is the brightest ion emission from the plasmasphere which is proportional to the He^+ column abundance. The EUV sensor contained in the American IMAGE satellite which was launched in 2000 studied the distribution of cold plasma in the plamasphere by imaging the distribution of the He^+ ion for about five years[3-5].

Although the EUV Imager data only showed the maps of two dimensional column density of the plamasphere, the relation (Fig. 1) between the CT technique and the plasmaspheric EUV Imaging provides the possibility of reconstructing the three dimensional density distribution of the plasmasphere by using the CT method[4-6].

In this paper, a three dimensional (3-D) model for the density distribution of the plasmasphere is established. We also simulated the imaging process of EUV sensor and obtained the simulated the EUV data sampled along a circular orbit with radius of 60Re. The shelter problem which exists in the reconstruction by using real data is also considered in the above-mentioned simulation, and a modified ART reconstruction method was devised to resolve it.

Received: 2009-10-27; revised: 2010-01-05

* Supported by the National Natural Science Foundation of China (Nos. 10575059, 60871084, and 10905030)

** To whom correspondence should be addressed.
E-mail: lliang@tsinghua.edu.cn; Tel: 86-10-83186049

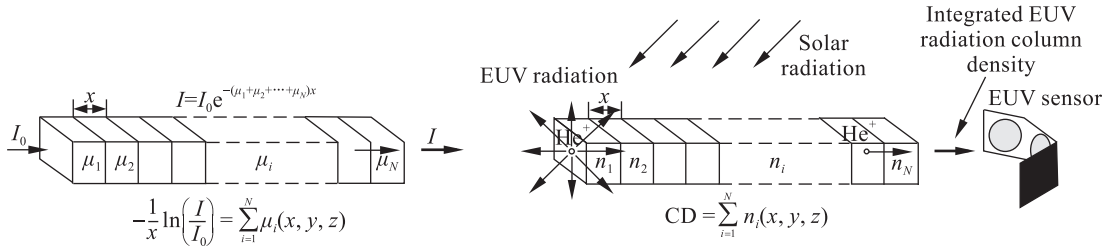

Fig. 1 Illustration of the relation between CT technique and the plasmaspheric EUV imaging

1 3-D Plasmasphere Phantom

1.1 Simulation data

After an analysis of the real data sampled by the IMAGE satellite, we find that the EUV sensor only took 60 'photos' within an approximate 90-degree scanning range. These data do not satisfy the data sufficiency condition for exact CT reconstruction. Furthermore, the sun, the earth and the plasmasphere are always moving during the EUV data acquisition. If we directly reconstruct the plasmasphere from these incompleted real data without any other correction process, the reconstructed images will be extremely corrupted by the artifacts. Since the first step of our project is to prove that the CT technique is available to study the global density distribution of the plasmasphere, we need simplify our mathematical and physical model in order to eliminate other impact factors. Otherwise, we cannot distinguish the bad reconstructed image due to the incomplete data problem or the wrong premise. Based on the validation of the fundamentals, further studies will be focused on the other problems like incomplete data, motion and so on.

1.2 3-D plasmasphere phantom

We suppose the density of the plasma within the phantom is uniform and equals 1. The boundary is defined as Eq. (1) in the slice which parallels the solar direction and passes through the geomagnetic axis of the earth. The expression is given in the polar coordinates with the origin located at the center of the earth[5].

$$r = 4\,\mathrm{Re}\cos^2\Phi \tag{1}$$

The expression suggests that the farthest point of the boundary is 4Re from the earth's center. Converting the polar coordinates to the Descartes coordinates and rotating the slice around the z-axis, obtain the 3-D phantom of the plasmasphere with the boundary expressed by

$$Z^2=(4\mathrm{Re})^{2/3}(X^2+Y^2)^{2/3}-X^2-Y^2 \tag{2}$$

Between the plasmasphere and the earth is the ionosphere in which the density of He^+ equals 10 times that of the density of He^+ in the plasmasphere.

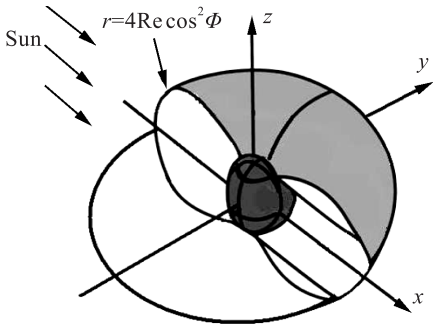

Fig. 2 Illustration of the 3-D plasmasphere phantom

Actually, the real contribution of the plasmasphere is much more complex than the above phantom. When reconstructing the plasmasphere using the simulation data instead of the real data, there is a question raised as to whether or not the result can verify our formula for the reconstruction of the plasmasphere. The answer is yes. Once the reconstruction algorithm is validated, it can also be used to reconstruct the plasmasphere from the real data, because the physical process of the simulation data is the same as for the EUV sensor. The difference is that more reconstruction skills and correction methods are needed when dealing with the real data.

1.3 Computer-simulated data

Based on the above 3-D plasmasphere phantom, we computer-simulated the imaging process of the EUV sensors on the IMAGE satellite. It was known that the brightness of each element of the EUV image is proportional to the integral column density of He^+ in the corresponding direction. In order to get the phantom projection along a certain line, we need to

calculate the integrated column density of all parts of the phantom along this line. The main processes are as follows:

(1) Define the starting point (the position of the sensor) and the direction (detecting direction of the sensor) of a ray;

(2) Calculate the integrated column density along the ray until reaching the boundary of the earth or passing through the region of the phantom;

(3) Record the integral value in the corresponding element of the 2-D projection image matrix.

It can be imagined that there is no EUV emission in four regions: the earth region, the region between the ionosphere and the earth, the earth shadow zone, and the region outside the phantom (Fig. 3).

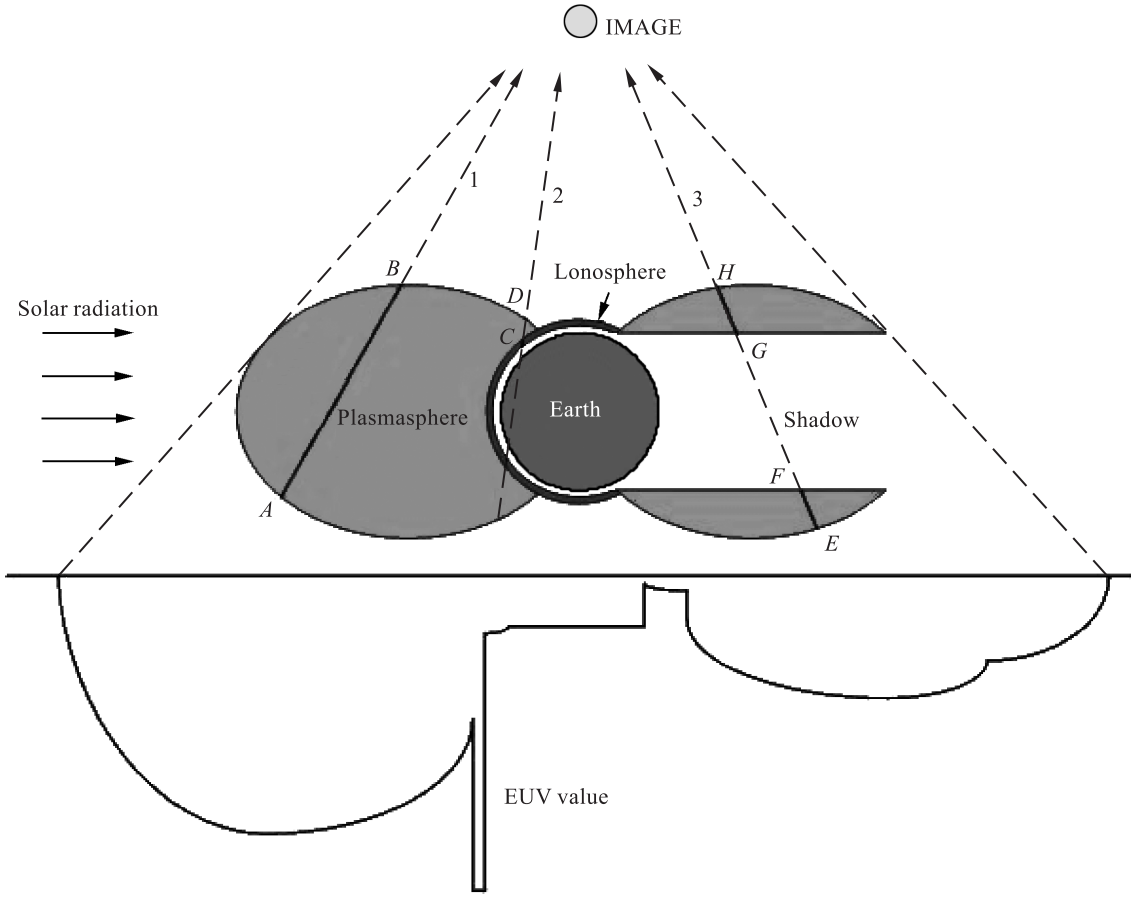

Fig. 3 Illustration of structures of the plasmasphere phantom

2 3-D Cone-Beam Reconstruction

2.1 Algebraic reconstruction techniques

As mentioned in Section 1, the data from the EUV sensor is incomplete for the CT reconstruction due to the limited-angle and the earth absorption problem. Based on many comparisons, the algebraic reconstruction technique (ART) algorithm can provide much better results than the other filtered-backprojection (FBP) type algorithms. As a brief review, the ART procedures are as follows:

(1) Give an initial estimation $f^{(0)}$;

(2) Produce $f^{(k+1)}$ from $f^{(k)}$ by Eq. (3);

$$\begin{cases} f^{k+1} = f^{k}, & \| \boldsymbol{H}_i \|^2 = 0; \\ f^{k+1} = f^{k} + \lambda^{k} \dfrac{g_i - \boldsymbol{H}_i f^{k}}{\| \boldsymbol{H}_i \|^2} \boldsymbol{H}_i^{\mathrm{T}}, & \| \boldsymbol{H}_i \|^2 \neq 0 \end{cases} \tag{3}$$

(3) Stop the iteration until $f^{(k)}$ satisfies the convergency condition.

Note that, we only need to consider a single ray in each iterative step. That is, only the pixels intersected by the number k ray changed while $f^{(k+1)}$ was produced from $f^{(k)}$.

Where g^i is the projection of number i ray, and $\boldsymbol{H}_i$ is the number i vector of the projection matrix $\boldsymbol{H}$, $\boldsymbol{H}$

provides two types of information for the iteration: (1) which pixel is intersected by the i ray (The index of the element which does not equal 0); (2) the contribution of each pixel (the value of the corresponding element). The correction on each iteration step should be proportional to both the distance $g^i - \boldsymbol{H}_i f^k$ and to the value of $\boldsymbol{H}_i$. The relaxation parameter λ^k is used to control the convergence speed[7].

2.2 Modified ART method

In this section, a modified ART reconstruction method is proposed according to the characters of EUV imaging. The first problem is that the earth absorbs all the electromagnetic radiation passing through it, which has two effects. One effect is that the earth absorbs the EUV emission behind the earth and only the radiation between the earth and the sensor is detected (Line 2 shown in Fig. 3). The other effect is that the earth absorbs the solar radiation and the He^+ in this shadow zone does not scatter EUV radiation (Line 3 shown in Fig. 3). To deal with this problem, the elements were assigned 0 in these shelter regions of H, which means the elements in such regions make no contribution to the EUV imaging. In this paper, we assumed the shadow zone would not change during the EUV data acquisition.

A non-negative constraint is also used in each iterative step. The elements with negative value are assigned to 0 because the distribution of the plasmasphere is always non-negative.

3 Numerical Experiments

The real IMAGE orbit is an ellipse with its perigee inside the plasmasphere. The EUV sensor only works outside the plasmasphere. Here, we chose a circle orbit with the radius of 60Re for a panoramic view of the plasmasphere instead of the real one. The EUV projections covering 360 degrees were sampled at a rate of $\Delta\theta = 2\pi/360$, with 200 ray sums per projection for a field-of-view (FOV) of radius 4.3Re. The reconstructions are achieved on a grid of 128^3 cubic pixels. The modified ART method mentioned above was used for this reconstruction.

Three projection images of the phantom are shown in Fig 4. Figures 4a-4c simulate the EUV images along the observation direction of the $-x$-axis, $+z$-axis, and $+x$-axis, respectively. The gray part is the plasmasphere while the white part is the ionosphere. The earth shadows due to the earth-absorption effect are also shown in these pictures.

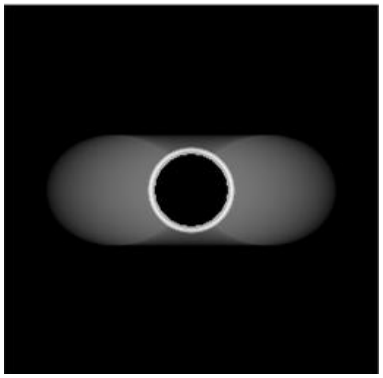

(a)

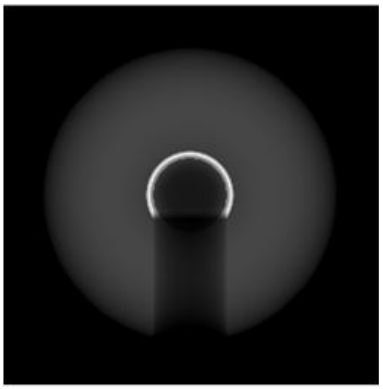

(b)

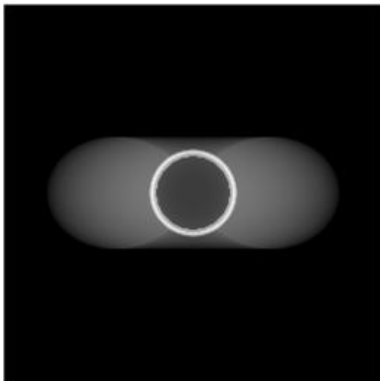

(c)

Fig. 4 Illustration of projection images of the plasmaspheric phantom, (a) along the observation direction of the $-x$-axis, (b) along the observation direction of the $+z$-axis, and (c) along the observation direction of the $+x$-axis

Figure 5a shows the image of the 3-D rendering result of the reconstruction. We find that the result corresponds with the phantom very well since the data in 360-degree was used. Figures 5b-5d show three orthogonal slices of z=0, x=0, and y=0, respectively. They

also correspond well with the phantom. Figures 5e and 5f show the profiles at the horizontal and vertical lines in Fig. 5d. We find that the reconstruction values are quite accurate both in the plasmasphere and ionosphere. Moreover, we also reconstructed the phantom using the data within a 180-degree range for comparison, where the data sufficiency condition was not satisfied. The reconstruction results are shown in Fig. 6, including the 3-D rendering result image, three orthogonal slices images and two profiles at the same lines as Fig. 5.

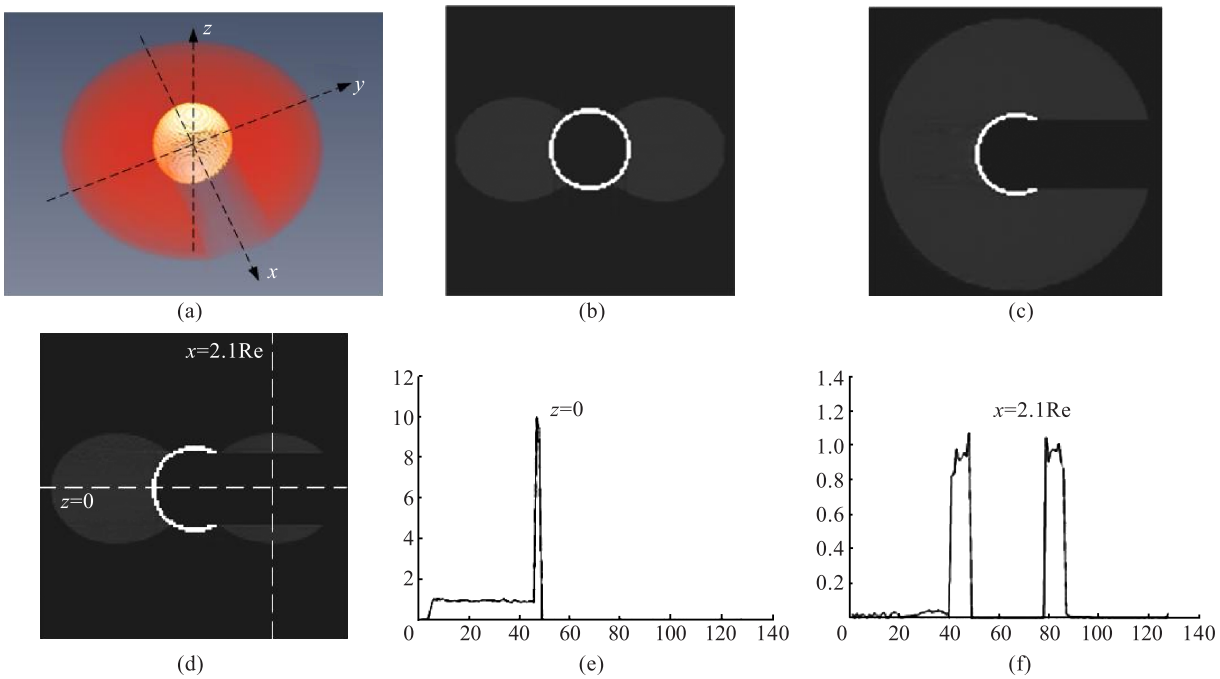

Fig. 5 Illustration of reconstruction result using 360-degree data. (a) 3-D rendering result. (b), (c), and (d) are the slice at *x*=0, *z*=0, and *y*=0 planes, respectively. (e) is the profile along horizontal line in (d). (f) is the profile along the vertical line at *x*=2.1Re in (d).

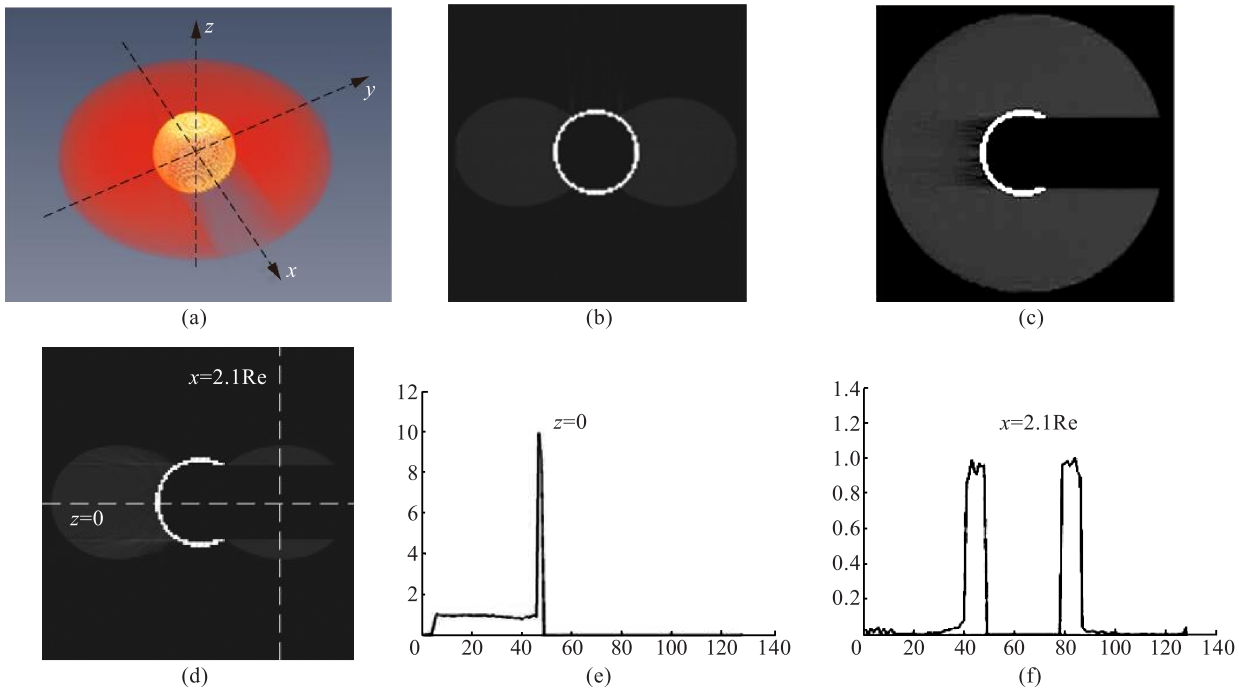

Fig. 6 Illustration of reconstruction result using 180-degree data. (a) 3-D rendering result. (b), (c), and (d) are the slice at *x*=0, *z*=0, and *y*=0 planes, respectively. (e) is the profile along horizontal line in (d). (f) is the profile along the vertical line at *x*=2.1Re in (d).

Comparing with Fig. 5, there is only a little difference between these two groups of reconstructed images. It suggests that the modified ART method can provide pretty good reconstruction results from the data covering only a 180-degree scanning range.

4 Conclusions

In this paper, we simulated the cone-beam imaging processes of the EUV imager. From the numerical results, we know the modified ART method can provide pretty good reconstruction images using the data within 360 degrees and 180 degrees. It can be concluded that it is feasible to use the CT technique to analyze the data collected by the EUV sensor on the IMAGE satellite. The CT technique provides an approach to achieve the 3-D density distribution of the plasmasphere. Our future studies will be focused on the 3-D cone-beam reconstruction of the plasmasphere using the real data from the IMAGE satellite. Considering the limited-angle (about 90 degrees) problem, more a priori knowledge may be used to improve the modified ART algorithm in areas such as boundary constraint, and motion compensation.

References

[1] Burch J L. IMAGE mission overview. *Space Science Reviews*, 2000, **91**(1-2): 1-14.

[2] Burch J L. Magnetospheric imaging: Promise to reality. *Reviews of Geophysics*, 2005, **43**(3): RG3001.

[3] Sandel B R, Broadfoot A L, Curtis C C. The extreme ultraviolet (EUV) investigation for the image mission. *Space Science Reviews*, 2000, **91**: 197-242.

[4] Xu R L, Huang Y, Li L, et al. Deduction of the global density of earth plasmasphere from the model column density of the plasmasphere using computed tomography technique. In: Proceedings of the 37th COSPAR Scientific Assembly. Montreal, Canada, 2008.

[5] Li L, Chen Z Q, Xu R L, et al. A study of the plasmasphere density distribution using computed tomography methods from the EUV radiation data. *Advances in Space Research*, 2008, **43**: 1143-1147.

[6] Li L, Chen Z Q, Xu R L, et al. A weighted FBP reconstruction for plasmasphere CT imaging. In: Proceedings of 2008 IEEE Nuclear Science Symposium. Dresden, Germany, 2008: 5086-5089.

[7] Zhuang T G. Principle and Algorithm of Computed Tomography. Shanghai: Shanghai Jiaotong University Press, 1997. (in Chinese)